PHYSICAL REVIEW A VOLUME 24, NUMBER 5 NOVEMBER 1981

Charge-exchange excitation and recombination of oxygen in the ISX-*B* tokamak

R. C. Isler, L. E. Murray, S. Kasai,* J. L. Dunlap, S. C. Bates,
P. H. Edmonds, E. A. Lazarus, C. H. Ma, and M. Murakami
Fusion Energy Division, Oak Ridge National Laboratory, Oak Ridge, Tennessee 37830
(Received 12 June 1981)

Several spectral lines produced by charge transfer of neutral-beam hydrogen atoms with completely ionized oxygen have been detected in the impurity studies experiment *B* (ISX-*B*) tokamak, and have been used to compute the absolute concentrations of O^{8+}. Charge-exchange recombination is found to have a minor effect on the total radiative losses, but enhanced transport during neutral-beam injection appears to raise the oxygen radiation from the interior of the discharges by factors of 3 to 5. This result may reflect an increase of anomalous transport rates that could account for the density "clamping" often observed with injection.

I. INTRODUCTION

One of the difficulties of studying the concentrations and the transport of light impuritities in tokamaks has been the general inability to observe the completely ionized species which are often dominant in the center of the discharge. It is known, however, that charge exchange between hydrogen and highly stripped impurities takes place into excited states, e.g.,

$$H^0+O^{8+}\rightarrow H^+ +(O^{7+})^* , \quad (1)$$

and the subsequent radiation can provide a means for following the fully ionized stages. Reactions typified by Eq. (1) are termed charge-exchange excitation. Signals from this process were observed from oxygen in the ORMAK (Oak Ridge tokamak) device where the neutral heating beams provided the source of hydrogen,[1] and from carbon in the *T*-4 tokamak where an active diagnostic beam was employed.[2] No attempt was made to calculate the oxygen concentrations from the ORMAK observations, mainly because the partial cross sections for exciting the various n and l states were not known. Since that time, these individual cross sections for hydrogenic ions have become available,[3,4,5] and this paper describes how they have been utilized to measure the fully ionized oxygen concentration in the ISX-*B* tokamak.

Analysis of lines excited by charge-exchange excitation may provide the only efficient method of evaluating the influence of auxiliary heating or the effectiveness of a divertor on light impurities. The line intensities of the normally radiating species are sensitive to the cross field transport, and in many experiments, one cannot tell without well resolved spatial measurements whether changes of radiation reflect changes of this transport or whether the impurity concentrations have actually been altered. We show in Sec. III that if the neutral-beam parameters and the excitation cross sections are well known, a satisfactory determination of the O^{8+} content can be made from the charge-exchange signals.

Another aspect of charge transfer that has been closely scrutinized lately is its effectiveness as a recombination mechanism.[6,7] This process increases the steady-state fraction of the incompletely ionized species of light impurities in the center of the plasma during neutral-beam injection, and as a consequence, the radiative power losses from electron excitation are augmented.[8] It has been suggested that electron excitation following charge-exchange recombination,

$$e+O^{7+}\rightarrow e+(O^{7+})^* , \quad (2)$$

is responsible for the failure to heat electrons in the DITE tokamak (diverted injected tokamak experiment) under certain conditions.[9] The magnitude of this problem is also assessed for ISX-*B* in the present paper by analyzing radiation from O^{7+} ions. We conclude that it does not lead to large power losses. Indeed, we have usually observed significant electron heating up to injection powers of 1 MW. Although the O^{7+} radiation does increase during injection, it does not appear possible

to assign this behavior to charge-exchange recombination or to an impurity influx. Instead, more rapid particle circulation seems to be the cause. This conclusion also differs from the interpretation of recent results from the PLT (Princeton Large Torus) tokamak that indicate charge-exchange recombination is responsible for a strong increase of the Fe XXIV radiation during injection.[10] However, there are significant differences in the discharge characteristics of PLT and ISX-*B*, and the interpretations of the data are not necessarily contradictory.

II. EXPERIMENTAL ARRANGEMENT AND OBSERVATIONS

Two neutral-beam injectors are installed on ISX-*B*, each of which can provide over 1 MW of power into the plasma. The full energy component of the hydrogen atoms is usually between 30 and 40 keV (100-A sources). The best present analysis indicates that the fractional currents associated with the full, the one-half, and the one-third energy components of the beams are 0.60, 0.20, and 0.20, respectively.[11] Both beams are injected in the same direction as the plasma current (co-injection). The experiments discussed here have been carried out using hydrogen beams and deuterium plasmas.

A top view of the tokamak, the beamlines, and some of the diagnostic devices is shown in Fig. 1.

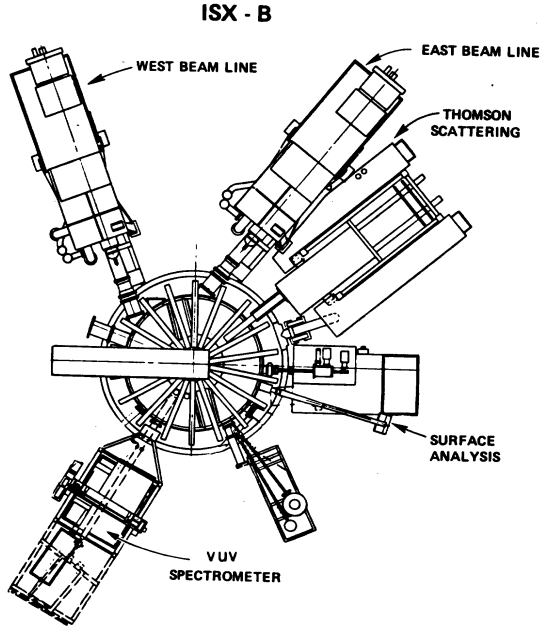

FIG. 1. Schematic view of ISX-*B* showing locations of the grazing incidence spectrometer and the two neutral-beam injectors.

The grazing incidence monochromator (McPherson Model 247) used for the line-integrated spectral observations is situated so that its field of view includes high energy hydrogen atoms from the west beam, but not atoms from the east beam. When the west beam is operated alone, the spectral signals observed result from the sum of charge exchange and electron excitation. But because the lifetime of the pertinent excited states are so short (less than 2×10^{-10} s), ions excited by charge exchange with the particles of the east-beam decay before they move along the toroidal magnetic field into the field of view of the spectrometer. As a result, when only the east beam is operating, the spectral radiation observed arises solely from electron-excitation (charge transfer with the ambient, thermalized deuterium which recycles from the wall or limiter can be neglected). This excitation should be toroidally uniform for the highly ionized stages because the transit time around the machine [$(5-8)\times10^{-5}$ s] is much shorter than the characteristic time for electron ionization [$(1-2)\times10^{-3}$ s].

The experimental arrangement shown in Fig. 1 allows the direct charge-exchange signal to be separated from the total signal by operating the beams at the same current and subtracting an "east-beam shot" from a "west-beam shot". The location of the spectrometer has one drawback. It is rather far downstream from the throat of the injector, and the H^0 current is severely attenuated before it crosses the field of view. Operation at plasma densities lower than usual have been required to do the studies described here.

Two experimental sequences have been examined. The discharge conditions and some qualitative aspects of the spectral data are discussed before presenting the detailed analysis for obtaining the oxygen concentrations. Several plasma parameters from sequence 1 (Figs. 2–5) are shown as a function of time in Fig. 2. The steady-state current is 160 kA, and the toroidal field is 12.3 kG. Deuterium is added to the machine throughout the shot causing the electron concentration to rise steadily. The injectors are turned on from 78 to 180 ms, at which time the current begins to run down, and the discharge terminates. The envelope of the magnetohydrodynamic (MHD) signal and the soft x-ray signal are also shown in Fig. 2 to facilitate comparison of the temporal evolutions with the other traces. Because the basic data acquisition rate is one point per millisecond, variations occurring on a shorter time scale are not reproduced in

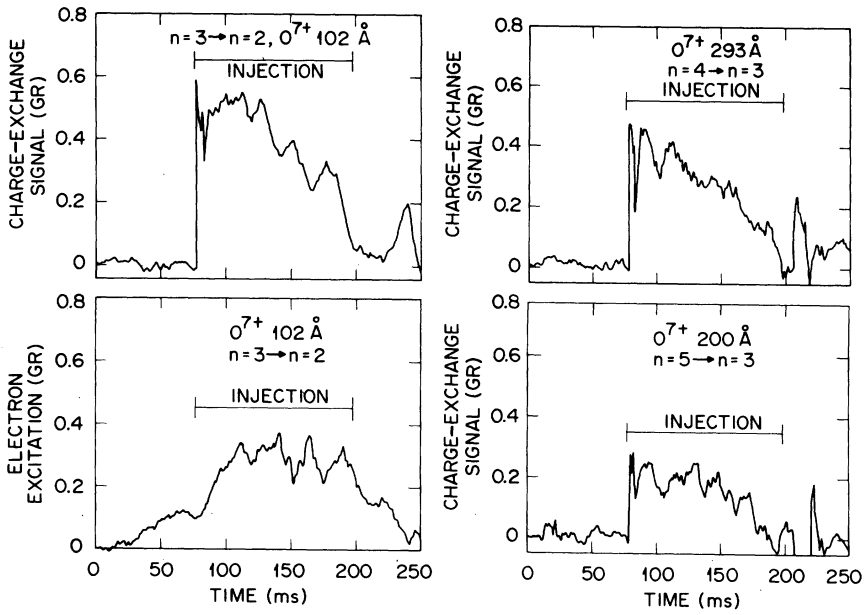

FIG. 5. Emission rates of O^{7+} ions during sequence 1.

value following the start of the beam pulse, and if an average is taken through the large-amplitude oscillations, the signal level decreases only slightly until the discharge is terminated. It will be shown in Sec. IV that the rise of the electron-excited signal must be caused by some process other than charge-exchange recombination.

The second sequence (Figs. 6–8) has not been documented so well as the first, nor are the operating conditions as favorable for analyzing the spectral data. Nevertheless, the line radiation provides a great deal of information concerning the oxygen behavior during injection. The plasma parameters are illustrated in Fig. 6. The nominal plasma current and the toroidal field are 152 kA and 14 kG. The beam power is about 800 kW, and the timing of the west beam is shown in Fig. 6. Unfortunately, the onset of the east-beam pulse occurs 10 ms earlier. The charge-transfer signals obtained by subtracting the data from two shots are somewhat distorted because of this difference, but the most important aspects are still evident. In this sequence, the MHD level typically builds up slowly, and although oscillographs show high frequency precursers on the sawtooth oscillations, they are much more regular and lower in amplitude than those observed in sequence 1. The spectral line data are shown in Figs. 7 and 8. The time constant of the amplifier was 3 ms, so the rise of the initial spike appears slow and its amplitude is somewhat attenuated. Because of the difference in timing, we show the individual signals using the east beam and the west beam, as well as the difference which provides the charge-exchange signal. Analysis of this difference signal to obtain the O^{8+} concentration should be slightly influenced by the timing offset at the beginning of the injection period when the east-beam signal is low or at the end when a quasistationary state is reached. But the decay of the 3→2 transition after the initial rise

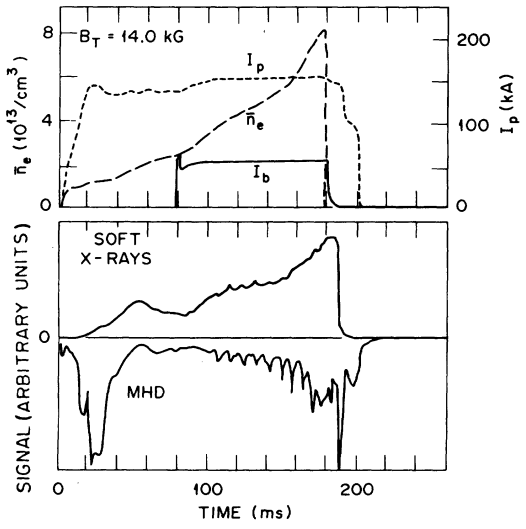

FIG. 6. Temporal behavior of several plasma parameters for sequence 2. I_p and $\bar{n}_e$ are the plasma current and the line averaged electron density. The total beam current I_b is 24 A.

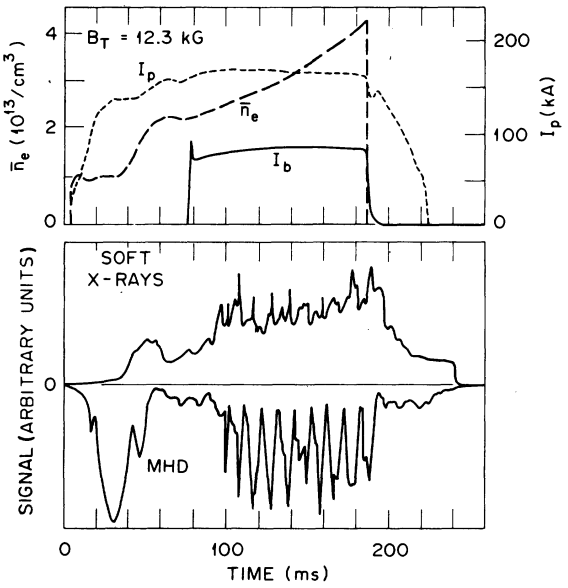

FIG. 2. Temporal behavior of several parameters for sequence 1. I_p and $\bar{n}_e$ are the plasma current and the line-averaged electron density. The total beam current I_b is 36 A.

Fig. 2, so oscillographs of the MHD and of the soft x-ray signals are also presented in Fig. 3 to better illustrate the fluctuations. It is seen that during injection, periodic bursts of high-frequency MHD activity occur coincidentally with low-frequency sawtooth activity. It has been proposed that this phenomena may be caused by the nonlinear coupling of $m=1$ and $m=2$ modes and the possible development of ergodic regions in the plasma.[12]

Electron temperature and density profiles were taken at 140 ms into the discharge. These are shown in Fig. 4. The temperature profile is relatively flat in the center with a maximum near 1150 eV. Profiles were not obtained for the preinjected plasma, but the sequence immediately preceding the one we describe here employed only

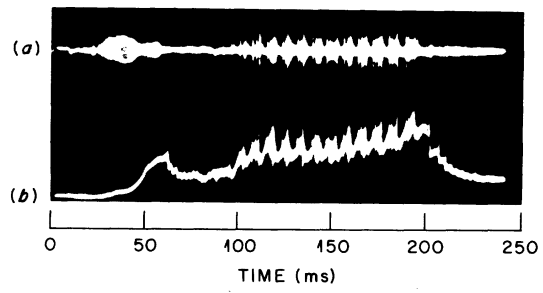

FIG. 3. Oscilloscope photographs of the soft x-ray and of the MHD signals for sequence 1.

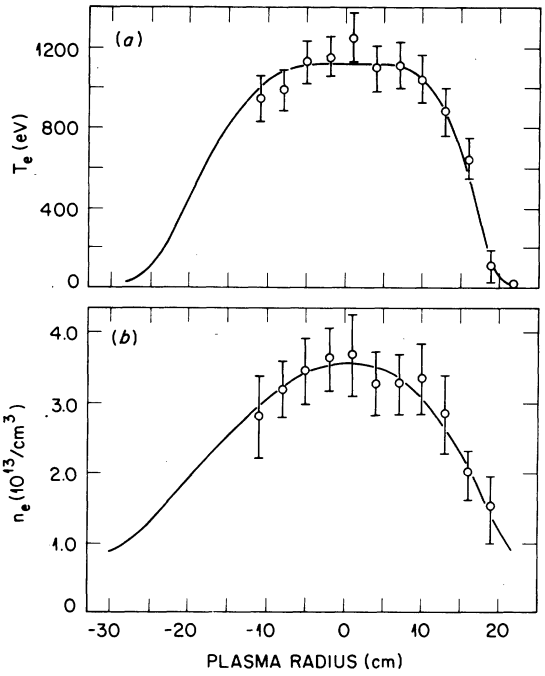

FIG. 4. (a) Plasma temperature and (b) density profiles for sequence 1.

ohmic heating, and the central temperature was 730 eV. We have assumed that this is a close approximation for the injection sequence just before the beam is turned on.

The emission rates[13] for lines of O VIII are illustrated in Fig. 5. Traces which are specified as electron excitation are east-beam shots, and those noted as charge-exchange excitation are obtained by a subtraction of two signals as we have described. These data have been numerically smoothed over 10-ms intervals except for the charge-exchange signals around the time of injection, 78 ms, where the normal 1-ms sampling rate was preserved in order to demonstrate the characteristic rapid rise. The initial spike and the following relaxation correspond to the same features that are present in the beam current pulse (Fig. 2). The rising plasma density and the concomitant attenuation of the beam before it crosses the field of view of the spectrometer cause the decrease of the charge-transfer signals after 120 ms. These data represent the first confirmation that several lines of oxygen produced by charge-exchange excitation can be observed during neutral-beam injection. As a result, our identification of this process is greatly strengthened. In contrast to the 1—2-ms rise in the charge-exchange signal, the electron-excited radiation requires about 30 ms to attain its peak

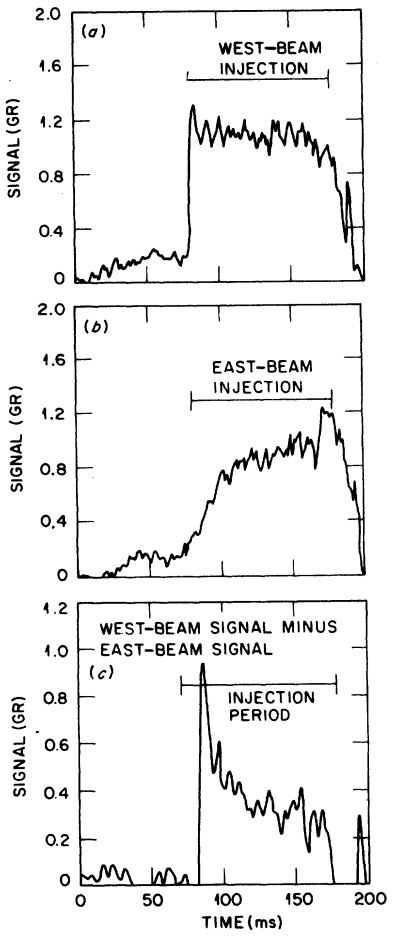

FIG. 7. Comparison of the $n=3\rightarrow n=2$ transition of O^{7+} when injection is only from the east or only from the west beam. The difference signal is from charge exchange alone.

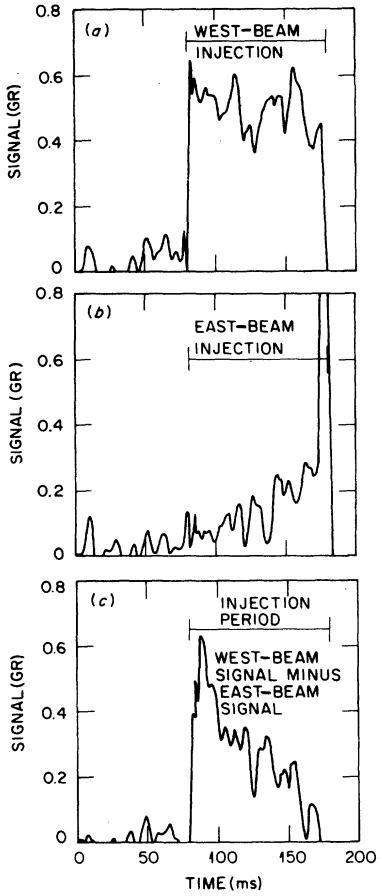

FIG. 8. Comparison of the $n=5\rightarrow n=4$ transition of O^{7+} when injection is only from the east or only from the west beam. The difference signal is from charge exchange alone.

is faster than if the beam timing had been the same. The $5\rightarrow 4$ transition is not so strongly influenced since its electron-excitation rate is only 20% of the $3\rightarrow 2$ rate, but its charge-exchange excitation rate is 70% of the $3\rightarrow 2$ rate.

III. ANALYSIS OF CHARGE-EXCHANGE EXCITATION

The analysis of the spectroscopic data will be discussed in three stages. First, we outline the method for obtaining the concentrations of completely ionized oxygen. Next, by using some simple anlaytic computations, the effect of charge-exchange recombination on the electron-excited signal is shown to be small. Finally, we discuss the computor simulation that is used in evaluating the oxygen ion concentrations from spectral emissions.

The results of this simulation indicate that oxygen ions, at least in the center of the plasma, circulate at a higher rate during injection than during ohmic heating.

The concentration of O^{8+} in the center of the plasma is determined from the charge-exchange signals through the relationship,

$$S_c=\sum_{k=1}^{3}\int_{-a}^{a} j_k(r)n_8(r)\sigma_E^k \mathrm{d}r\ . \tag{3}$$

Here, S_c is the measured emission rate of a spectral line, j_k is the current density of a given energy component of the neutral beam, and σ_E^k is the cross section for excitation of the line at a collision energy E_k. A 20% correction is added to the nominal value of the beam current to account for the low-energy neutral deuterium atoms (halo neutrals) which are formed by charge exchange of plasma

ions with the beam and which can subsequently charge exchange with the impurities. The integral of Eq. (3) is evaluated along the optic axis of the spectrometer by using assumed O^{8+} profiles and current densities based on known beam characteristics.

The total effective cross sections for charge-exchange excitation of a given spectral line are derived from the individual charge-transfer cross sections for populating specific n and l states of the hydrogenlike oxygen after taking account of all the branching and cascading in the decay process. Salop's[3] charge-transfer results are employed to compute the excitation cross sections listed in Tables I and II. Where necessary, these are extrapolated linearly to obtain the values for the full and the one-half energy components of the beam. The cross sections for the one-third energy component of the beam are assumed the same as for the one-half energy component. Uncertainties in the extrapolations do not strongly influence the analysis, since about 70% of observed excitation occurs from the primary energy component. Excitation takes place principally into the high angular momentum states of the $n=4$ and $n=5$ levels. As a result, a large fraction of the decay takes place through an yrast series, and the $\Delta n=1$ transitions between low levels, such as $n=3\rightarrow n=2$, come from cascades. In Table III we list the comparisons between the measured and the calculated relative intensities at 115 ms into the discharges. The comparisons must be considered satisfactory in view of the uncertainties in the calibration of the spectrometer, a factor of 1.5, and of the fluctuations in the charge-exchange signals.

The unattenuated neutral beam is represented by a Gaussian profile which is truncated by the entrance aperture into the tokamak. This profile is taken to be the same as the one determined by calorimetric measurements[14] downstream from the aperture when the previous 60-A sources were installed. The angular divergence is also known from prior investigations.[15] By using the coordinate system shown in Fig. 9, the unattenuated beam in the midplane of the torus is written as

$$j_k'(x,y)=\frac{I_k}{\pi}\left[\frac{D}{(D+\chi\tan\alpha_0)b_0}\right]^2\left[1-\exp\left[-\frac{D^2}{b_0^2}\right]\right]^{-1}\exp\left[-\left[\frac{(y-\delta)D}{b_0(D+\chi\tan\alpha_0)}\right]^2\right], \tag{4}$$

where I_k is the total neutral particle current at energy E_k, D is the radius of the entrance aperture (14 cm), χ is the distance from this aperture to the point of observation, b_0 is the $1/e$ point of the current profile (8.4 cm) at the entrance aperture, and δ is the offset of the center of the beam from the x axis (17 cm). Because of the finite extent of the aperture, the Guassian distribution is truncated at $(D+\chi\tan\alpha_0)$, where $\alpha_0(2.3°)$ is the angle or divergence at the outer edge of the beam. Figure 9 shows the approximate location of the beam particles in the midplane of the tokamak; the inner wall of the chamber intercepts a portion of the beam.

Equation (4) must be multiplied by a factor for the decay of the neutral beam as it passes through the plasma in order to obtain the expression for $j_k(r)$ in Eq. (3). The attenuation comes from ionization by electrons and from charge exchange and ionization by thermal protons. It is a reasonable approximation to neglect corrections for attenuation by impurities if their concentrations are small, and the factor can be written as

TABLE I. Effective excitation cross sections in units of 10^{-15} cm^2 for spectral lines produced by charge transfer of hydrogen on completely ionized oxygen at 32 keV. The calculations of Salop (Ref. 3) have been used.

n (lower level) \ n (upper level)	2	3	4	5	6
1	2.52	0.18	0.12	0.07	0.06
2		1.98	0.33	0.21	0.07
3			1.64	0.44	0.08
4				1.28	0.19
5					0.54

TABLE II. Effective excitation cross sections in units of 10^{-15} cm^2 for spectral lines produced by charge transfer of hydrogen on completely ionized oxygen at 26 keV. The calculations of Salop (Ref. 3) have been used.

n (lower level) \ n (upper level)	2	3	4	5	6
1	3.00	0.20	0.09	0.05	0.02
2		2.39	0.46	0.18	0.02
3			2.07	0.49	0.03
4				1.60	0.09
5					0.52

$$G=\exp\left[-\int\left[n_e\sigma_e\frac{\langle v_e\rangle}{\langle v_k\rangle}+n_p\sigma_p^k\right]dl\right], \tag{5}$$

where the integration is along the path of any infinitesimal beam element. If we take the concentrations of electrons and protons to be equal, use an average electron ionization cross section, and employ an electron spatial distribution characterized by a parabolic term raised to some power m, Eq. (5) can be expressed as

$$G=\exp\left[-n_e(0)\left[\sigma_e\frac{\langle v_e\rangle}{\langle v_k\rangle}+\sigma_p^k\right]\times\int\left[1-\frac{r^2}{a^2}\right]^m dl\right]. \tag{6}$$

When m is an integer, the integral in Eq. (6) can be solved analytically.

It is not possible to obtain well localized measurements of O^{8+}, because the heating beam is so wide at the point of observation. A profile for the fully ionized species must be assumed to get a first order evaluation of S_c from Eq. (3). In Fig. 10 we have plotted calculated values of S_c for the $n=3\rightarrow n=2$ transitions with $n_8(0)=2.0\times10^{11}$ cm^{-3} and a total beam current of 42 A. Both a flat profile and a peaked profile,

$$n_8(\rho)=1.8\times10^{11}(1-\rho^2)^3+0.2\times10^{11},$$

have been assumed and two values of m, the electron profile parameter, have been investigated. At central concentrations in the mid-10^{13} cm^{-3} range, the different impurity profiles give about a 30% difference of signal.

The central concentration of the fully ionized oxygen is first estimated by using the curves of Fig. 10 for uniform distributions of O^{8+}. The result is then employed in the RECYCL code (Sec. V) which calculates profiles of various ionization stages of oxygen by using *ad hoc* impurity transport rates and measured electron temperature and density profiles. The calculated profiles for O^{8+} are then used in Eq. (3) to recompute $n_8(0)$. The two computations are iterated until they give consistent results for both the charge-exchange emission and the electron-excited emission of the O^{7+} lines.

IV. CHARGE-EXCHANGE RECOMBINATION

The radiation from charge-exchange excitation and from electron excitation following charge-exchange combination are obviously not independent. It is useful to examine the results of some simple calculations which relate the two processes in order to determine whether the rise in electron-

TABLE III. Comparison of measured and calculated charge-exchange signals normalized to the 3→2 transition of O^{7+}.

Transition	λ(Å)	Meas.	Calc. (32 keV)	Calc. (26 keV)
3→2	102	1.00	1.00	1.00
4→3	293	0.63	0.83	0.87
5→4	633	0.83	0.62	0.67
5→3	200	0.38	0.22	0.20

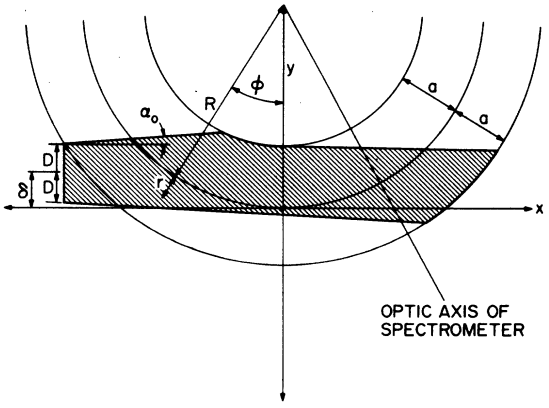

FIG. 9. Schematic diagram of midplane area through which particles from the west beam pass.

excited signals during injection is caused by recombination. The ISX-*B* plasmas always have central temperatures high enough to insure that O^{8+} and O^{7+} are the dominant ions in the center. Also, the ionization rate of O^{7+} is larger than all of the

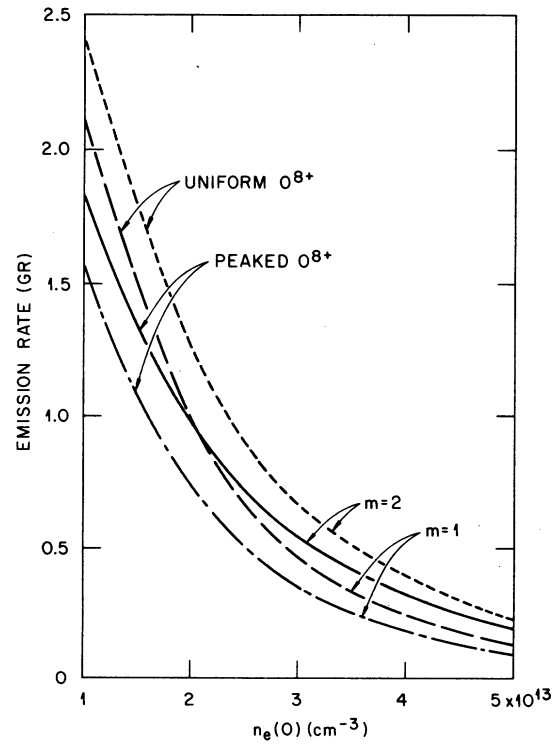

FIG. 10. Emission rate of the $n=3\rightarrow n=2$ transition of O^{7+} excited by charge exchange in the field of view of the grazing incidence spectrometer as a function of the central electron concentration. The fully ionized oxygen concentration on axis is 2.0×10^{11} cm^{-3} and the beam current is 42 A. Results for two profiles of O^{8+} and of n_e have been plotted.

recombination rates that would form O^{6+}. It is then reasonable to consider the oxygen as a two-ion system in the core of the plasma and to calculate the formation of O^{7+} from charge exchange on O^{8+}.

If transport is neglected and charge exchange is the major recombination mechanism, the detailed balance relationships are,

$$\dot{n}_8=-\beta n_8+\alpha n_7 , \tag{7}$$

and

$$\dot{n}_7=\beta n_8-\alpha n_7 , \tag{8}$$

where

$$\beta=\langle n_h\rangle v\sigma_T , \tag{9}$$

and

$$\alpha=n_e S . \tag{10}$$

The rate coefficient for ionization of O^{7+} is denoted by S, v is the velocity of the neutral-beam particles, σ_T is the total cross section for the charge transfer on O^{8+}, and $\langle n_H\rangle$ is the toroidal average of the hydrogen density of the beam. Equations 7 and 8 can be solved by employing the condition that the total oxygen concentration, n_τ, is constant,

$$n_\tau=n_8+n_7 , \tag{11}$$

The concentration of O^{7+} as a function of time is then

$$n_7(t)=n_\tau\frac{\beta}{\beta+\alpha}(1-e^{-(\beta+\alpha)t}) +n_7^0 e^{-(\beta+\alpha)t} , \tag{12}$$

where the initial concentration of O^{7+} is specified by n_7^0. For the conditions existing at the center of plasma during sequence 1, $\langle n_H(0)\rangle=2\times10^8$ cm^{-3}, $v=2.4\times10^8$ cm/s for the full energy component of the beam, and $\sigma_T=3\times10^{-15}$ cm^2, the reciprocal of the characteristic recombination time, β, equals 133/s. Immediately prior to injection the central plasma temperature and density are 730 eV and 3.6×10^{13} cm^{-3}, so that the value of α is 720/s. The solution of Eq.(12) is used to compute the relative time dependence of the 102-Å line emission following injection. It is shown in Fig. 11 for the center of the plasma by the curve labeled $r=0$. We have utilized the initial condition that $n_7^0/n_\tau=0.094$ which corresponds to a maximum net transport velocity of 1.1 cm/ms for O^{7+}. Impurity velocities of this magnitude are typically

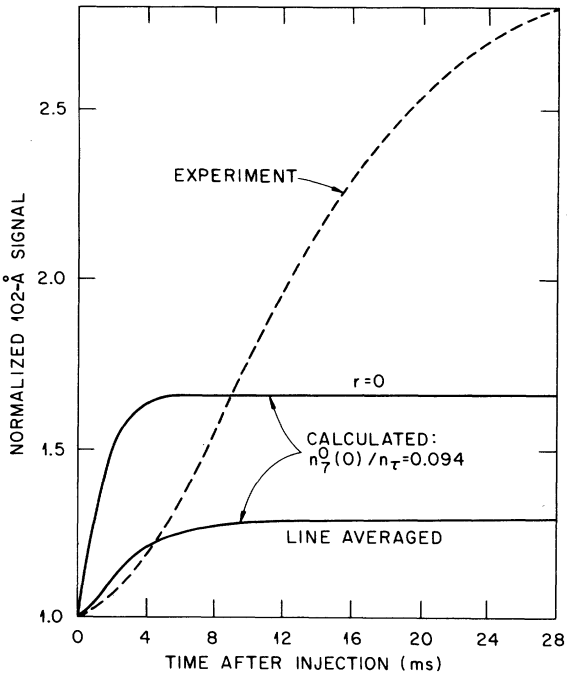

FIG. 11. A comparison between observed changes of electron-excited emission (O^{7+}, 102 Å) and changes calculated as a result of charge-exchange recombination. The curve labeled $r=0$ corresponds to central emission only.

detected in tokamaks[16,17] and are required in our modeling calculations (Sec. V) to explain the relative strengths of the excitation from charge exchange and from electrons at the onset of injection. The calculated rise time of the central radiation is much faster than the observed rate of increase, and the large difference provides a strong indication that recombination is not the sole reason for the change of electron-excited emission.

In order to effect a better comparison with the line-integrated spectral observations, a set of expressions similar to Eqs. (7)—(11) have been solved for the system of three ions by using the modeling from the RECYCL code to obtain the initial fractions of O^{6+}, O^{7+}, and O^{8+} as a function of radius prior to injection. The result is shown by the curve for line averaged emission in Fig. 11, where it is seen that 90% of the average contribution of charge-exchange recombination to the O^{7+} density should be apparent within about 8 ms after the beams are turned on. Although the rate of rise is slower than for the center alone, it still differs greatly from the experimental data.

Charge-exchange recombination appears to explain only a small fraction of the rise of electron-excited radiation during injection in ISX-*B* plasmas. The only alternative causes are an influx of oxygen during injection or increased transport rates so that inward diffusing O^{7+} is carried farther into the center of the plasma before burning out. In the next section we discuss these two possibilities and describe the modeling results using the RECYCL code.

V. MODELING CALCULATIONS

The final data analysis is performed by using the RECYCL code to model the oxygen in the plasma so that the computed values of both the charge-exchange excitation, and the electron excitation of the O^{7+} lines agree with experimental measurements. Briefly, this code performs a steady-state calculation in which impurities are assumed to be transported inward from the edge of the plasma, reverse direction at some point near the center, and are transported back to the edge. The inward and outward fluxes of the total oxygen content are individually conserved and have the same magnitude at every radius. The code is, quite clearly, not intended to reflect accurately the fundamental physics of the transport processes, but to represent them closely enough to provide a tool for the analysis of line-integrated spectral data. The impurity profiles and the transport velocities are adjusted in the code to give agreement with the experimental intensity measurements. Although the results are not unique, they are closely restricted in the present case by the requirement that both the calculated charge-exchange excitations and the electron excitations of the O^{7+} lines be consistent with the measurements.

Both uniform and peaked profiles of the oxygen concentration have been assumed for evaluating the present data. The transport rates in the RECYCL code are characterized by the average inward (or outward) impurity velocity, $\bar{v}_T$, between 4 and 12 cm. In Tables IV and V the results for central concentrations and for the 102-Å emission are compared for two assumed values of $\bar{v}_T$ at the onset of injection and for two values at 140 ms.

If a situation close to coronal equilibrium is assumed, for which $\bar{v}_T=0.1$ cm/ms, it is seen that the calculated electron-excited signal is too low by factors of 3 to 5. Agreement is realized if $\bar{v}_T$ is 1.9 cm/ms. This gives a maximum *net* inward transport velocity (*net* O^{7+} flux divided by concentration) of 1.1 cm/ms, which is consistent with the velocities observed when argon is puffed into ohmically heated discharges in ISX-*B*. The close agree-

TABLE IV. Measured emission rates (GR) for the 102-Å line of O^{7+}, and calculated rates for several modeling conditions. The total oxygen profile is assumed uniform. The O^{8+} concentration at $r=0$ is specified by $n_8(0)$, and the total oxygen concentration by $n_\tau(0)$.

	$n_\tau(0)$ (10^{11} cm^{-3})	$n_8(0)$ (10^{11} cm^{-3})	Charge-exchange excitation	Electron excitation
Initial injection (78 ms)				
Measured			0.58	0.10
Calculated				
$\bar{v}_T=0.08$ cm/ms	2.64	2.58	0.58	0.03
$\bar{v}_T=2.0$ cm/ms	2.85	2.57	0.58	0.10
During injection (140 ms)				
Measured			0.44	0.30
Calculated				
$\bar{v}_T=2.0$ cm/ms	2.80	2.52	0.44	0.14
$\bar{v}_T=6.9$ cm/ms	3.30	2.38	0.44	0.32

ment in Tables IV and V between the implied transport rates and the central concentrations shows that our conclusions do not depend strongly on the actual oxygen profiles.

A similar analysis is done for the plasma at 140 ms into the discharge when it has come to a steady state. If $\bar{v}_T$ is taken to be the same as during the turn-on phase, the electron-excited radiation is computed to be almost unchanged. However, the experimental value is actually a factor of 3 larger at 140 ms than at 78 ms (Fig. 5). In order to match the experimental results it is necessary to assume $\bar{v}_T = 6-7$ cm/ms, but to add less than a 20% increase in n_τ. No success has been achieved in attempting to model the experimental results by retaining $\bar{v}_T \simeq 1.9$ cm/ms and using total oxygen profiles that are peaked at the maximum of the electron excited O^{7+} radiation. The O^{7+} and O^{8+} ions are coupled too strongly by atomic processes to match both the charge-exchange excitation and the electron excitation in this manner.

The conclusion that the oxygen concentration in the center does not increase much during injection is strongly substantiated by the soft x-ray signal (Fig. 2). Modeling calculations indicate that this signal should rise by a factor of 2, between 78 and 140 ms, solely from the changes in T_e and n_e. The measured factor is 2.5 ± 0.5 where the uncertainty results from the amplitude of the sawteeth. If a change of oxygen concentration were the only

TABLE V. Measured emission rates (GR) for the 102-Å line of O^{7+} and calculated rates for several modeling conditions. A parabolic squared profile is assumed for the total oxygen content. The O^{8+} concentration at $r=0$ is specified by $n_8(0)$, and the total oxygen concentration by $n_\tau(0)$.

	$n_\tau(0)$ (10^{11} cm^{-3})	$n_8(0)$ (10^{11} cm^{-3})	Charge-exchange excitation	Electron excitation
Initial injection (78 ms)				
Measured			0.58	0.10
Calculated				
$\bar{v}_T=0.09$ cm/ms	3.04	2.96	0.58	0.02
$\bar{v}_T=1.9$ cm/ms	3.30	2.96	0.58	0.10
During injection (140 ms)				
Measured			0.44	0.30
Calculated				
$\bar{v}_T=1.9$ cm/ms	3.10	2.79	0.44	0.13
$\bar{v}_T=6.3$ cm/ms	3.80	2.72	0.44	0.31

cause of the rise of the electron-excited radiation from the 102-Å line, the soft x-ray signal would be expected to increase by a factor of 4—5, since the major contribution comes from radiative recombination into the light impurities, carbon and oxygen.

A detailed analysis of the data from sequence 2 is not warranted because the electron temperature and density profiles are not well documented. However, if the same relative profiles of the temperature and density and the same central values of the electron temperature are used as for sequence 1, the numerical analysis yields conclusions similar to those already presented; however, the absolute oxygen concentrations are twice as large and the value of $\bar{v}_T$ just before injection is 1.7 cm/ms rather than 2.0 cm/ms. We are again led to the inferrence that the oxygen density changes by less than 20% during injection, but that the transport rates are increased by a factor of 4—5.

VI. DISCUSSION AND SUMMARY

It appears quite feasible to detect completely ionized impurities from the charge-exchange excitation of these ions by neutral beams. Several spectral lines of O^{7+} have been observed, and within the experimental uncertainties, the relative intensities agree with the calculated values. Some insight into the absolute accuracy of the oxygen concentrations deduced from spectral data can be gained by comparing to other, nonspecific measurements of the impurity content. The plasma resistivity provides a value of the average ion charge, $\langle Z_{\text{eff}} \rangle$, and the soft x-ray signal comes mainly from bremsstrahlung and radiative recombination into light impurities. The oxygen contribution to $\langle Z_{\text{eff}} \rangle$ is calculated from the spectroscopic data to be 0.5 in the inner half of the plasma both before and during injection. Resistivity measurements indicate that the contribution from all impurities is 1.0. In most of our discharges we estimate that other impurities contribute roughly one-half the oxygen value. The poor quality of the loop-voltage signal and the uncertainty of spectrometer calibration can easily account for the 30% discrepancy between the spectroscopic and the resistivity measurements of $\langle Z_{\text{eff}} \rangle$. Similarly, the calculated soft x-ray signal, including only bremsstrahlung and recombination from hydrogen and from oxygen (as measured by spectroscopy), is one-half the observed value; the hydrogen contribution amounts to 31% of the total. But we expect bremsstrahlung and recombination from other impurities to contribute to the observed signal, and some fraction also results from x-ray line emission. The spectroscopic measurements appear to underestimate the oxygen concentration by 50% at most when compared with the resistivity and the soft x-ray signals. This accuracy is as good as can be expected from the present data; the combined uncertainties of the spectroscopic calibration, the beam parameters, and the theoretical cross sections is judged to be 60%.

The inference that the oxygen transport rates are increased by a factor of 3—5 during neutral-beam injection results from the fact that the O^{7+} and the O^{8+} concentrations are so strongly coupled by the atomic physics and the transport rates, that consistency of the charge-exchange excitation and the electron excitation cannot be realized by any other means when trying to model the data. The exact description of the transport is not obtainable from the line-integrated data nor from the RECYCL code. Only some measure of the average velocities can be achieved. Although the conclusion that the transport rates are altered rather severely by the injection is not affected by the uncertainity of the measured parameters, the values of tranport velocities required in the code do depend upon the beam current densities, $j_k(r)$, calculated along the observation chord. If the beam currents are actually lower than those we have used in the analysis, then the real O^{8+} concentration is larger than the computed values. As a result, a lower value of $\bar{v}_T$ can reproduce the electron excited emission. If we assume that the oxygen concentrations are 50% larger than those listed in Tables IV and V, the magnitudes of $\bar{v}_T$ necessary to match the injection and the pre-injection data are approximately $\frac{2}{3}$ the listed values.

The inferred increase in the oxygen transport during injection is consistent with two other features frequently seen in ISX-*B* discharges, the so-called density "clamp" and the prevalence of smaller values of $\langle Z_{\text{eff}} \rangle$ during neutral-beam injection than during ohmic heating alone. In ohimically heated plasmas the electron concentration is increased during the discharge by puffing gas into the edge of the plasma. If injection takes place into such a plasma, the electron concentration often "clamps" at a constant level and does not continue to rise. This behavior could be caused by the enhancement of an anomalous diffusion process increasing the transport rates and preventing the density from rising.

The differences in the resistivity and in the soft x-ray signals during ohmically heated and injection discharges can be interpreted similarly. We have already noted that $\langle Z_{\text{eff}} \rangle$ from the resistivity measurements equals 2 during injection. In the ohmically heated discharges that were documented just prior to the injection sequence, $\langle Z_{\text{eff}} \rangle$ equaled 4 at a comparable time during the shot. The soft x-rays also indicate this difference. In ohmically heated discharges in deuterium, the signal rises faster than the electron concentration increases,[18] implying that impurities are accumulating continuously in the center as if classical and neoclassical diffusion were dominating the transport. But it is seen that no such accumlation takes place during injection, and a possible explanation is that an anomalous diffusion mechanism becomes dominant for the oxygen, as well as for the electron transport. This process should not be confused with beam-driven, neoclassical flow reversal mechanisms which also stop the accumlation of minor impurities, but which do not necessarily affect the major impurities such as oxygen.[19,20] These processes have been observed in ISX-*B* when using lower injection powers so that the MHD levels remain small.[21] In such cases the electron excited O VIII radiation is observed to increase by only 50%, rather than by factors of 3–5, thus indicating a much smaller enhancement of the anomalous transport than observed in the present experiments.

In summation, a consistent interpretation of the present results can be constructed from the inference that the diffusion of oxygen in the center of the plasma is enhanced during injection. An explanation of the mechanism has not yet been formulated, but the very high transport rates required to explain the data may result from the growth of a large $m=1$ island and the development of stochastic regions generated by its nonlinear interaction with $m=2$ modes.[12]

ACKNOWLEDGMENTS

We would like to acknowledge the support and encouragement of J. Sheffield and M. Saltmarsh in performing these experiments. Special thanks are due to H. Ketterer, T. Rayburn, J. Yarber, and W. Redmond who kept ISX-*B* operating during this period. This work was sponsored by the office of Fusion Energy (ETM), U. S. Department of Energy under Contract No. W-7405-eng-26 with the Union Carbide Corporation.

---

*Visitor from the Japanese Atomic Energy Research Institute.

[1]R. C. Isler, Phys. Rev. Lett. 38, 1359 (1977).

[2]V. V. Afrosimov, Y. S. Gordeev, A. N. Zinoviev, and A. A. Korotkov, Zh. Eksp. Teor. Fiz. Pis'ma Red. 28, 505 (1978) [JETP Lett. 28, 500 (1978)].

[3]A. J. Salop, J. Phys. B 12, 919 (1979).

[4]R. E. Olson (private communication).

[5]V. A. Abramov, F. Baryshnikof, and V. S. Lisitsa, Zh. Eksp. Teor. Fiz. Pis'ma Red. 27, 494 (1978) [JETP Lett. 27, 465 (1978)].

[6]R. C. Isler and E. C. Crume, Phys. Rev. Lett. 41, 1296 (1978).

[7]V. A. Krupin, V. S. Marchenko, and S. I. Yakoblenko, Zh. Eksp. Teor. Fiz. Pis'ma Red. 29, 353 (1979) [JETP Lett. 29, 318 (1979)].

[8]R. A. Hulse, D. E. Post, and D. R. Mikkelsen, J. Phys. B 13, 3895 (1980).

[9]K. B. Axon *et al.*, in *Proceedings of the Eighth International Conference on Plasma Physics and Controlled Nuclear Fusion Research, Brussels, 1980* (International Atomic Energy Agency, Vienna, 1981), p. 413.

[10]S. Suckewer, E. Hinnov, M. Bitter, R. Hulse, and D. Post, Phys. Rev. A 22, 725 (1980).

[11]W. Gardner (private communication).

[12]J. A. Holmes, B. Carreras, W. A. Cooper, H. R. Hicks, V. E. Lynch, and K. E. Rothe, Bull. Am. Phys. Soc. 25, 931 (1980).

[13]All spectral emission rates are given in gigarayleighs (GR). 1 gigarayleigh $=10^{15}$ photons/cm^2 s.

[14]J. Kim (private communication).

[15]J. Kim and J. H. Whealton, Nucl. Instrum. Methods 144, 187 (1977).

[16]T. F. R. Group, Plasma Phys. 20, 735 (1978).

[17]T. F. R. Group, Phys. Rev. Lett. 36, 1306 (1976).

[18]R. C. Isler, S. Kasai, L. E. Murray, M. Saltmarsh, and M. Murakami, Phys. Rev. Lett. 47, 333 (1981).

[19]W. M. Stacey and D. J. Sigmar, Nucl. Fusion 19, 1665 (1979).

[20]K. H. Burrell, T. Ohkawa, and S. K. Wong, Phys. Rev. Lett. 47, 511 (1981).

[21]R. C. Isler *et al.*, Phys. Rev. Lett. 47, 649 (1981).

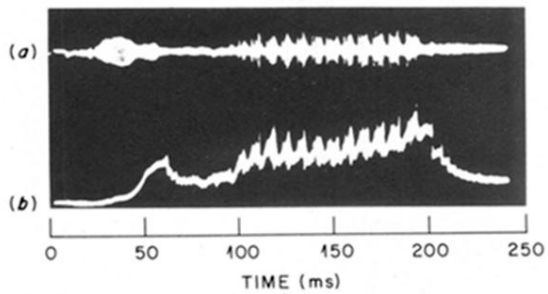

FIG. 3. Oscilloscope photographs of the soft x-ray and of the MHD signals for sequence 1.